PAPER

Check for updates

An efficient H_2O_2-based propylene to propylene oxide (HPPO) reaction catalyzed by ZnO/ZnO_2 materials†

Gebretinsae Yeabyo Nigussie, [ID] [abc] Yi-Fang Tsai,[a] Tsung-Cheng Yang,[d] Chia-Min Yang [ID] *[de] and Steve S.-F. Yu [ID] *[abc]

Propylene oxide (PO) is an essential feedstock in the plastic industry. Herein, unprecedented, inexpensive and robust zinc oxide (ZnO)-based catalysts were prepared. A ZnO nanorod (ZnO-NR) catalyst was synthesized using a solvothermal method. Another type of ZnO catalyst supported and immobilized on a mesoporous MCM-41 material (ZnO/MCM-41(x)) was also prepared with varied proportions ($x = 0.82–9.41$ wt%) of Zn content. The catalytic reactions of propylene epoxidation over ZnO-NR and ZnO/MCM-41(x) with H_2O_2 as an oxidant and acetonitrile as a solvent were studied at 30–70 °C and 5–20 bar. The ZnO catalysts were found capable of catalyzing the reaction with high H_2O_2 utilization and PO selectivity. Among them, ZnO/MCM-41(7.99) achieved nearly 100% PO selectivity and the highest turnover number of 124.4 (moles of PO per moles of Zn). The fresh catalysts, including ZnO-NR and ZnO/MCM-41(7.99), the spent catalysts, and the ZnO_2 nanoparticles were characterized by synchrotron powder X-ray diffraction, transmission electron microscopy, and X-ray absorption spectroscopy. The fractions of ZnO_2 in the spent catalysts were quantified to be higher than 50%. Electron paramagnetic resonance and X-ray photoelectron spectroscopy revealed that the ZnO_2 phase formed by reacting ZnO with H_2O_2 in acetonitrile, stored as green redox oxide materials, contained hydroperoxide, peroxide and superoxide species, which can be essential for catalytic production of PO. The observed ^{18}O enrichment in PO using $H_2^{18}O_2$ suggested that the reactive oxygenated species are generated from H_2O_2 and anchored on/in ZnO_2 for electrophilic epoxidation, with the assistance of acetonitrile.

1 Introduction

Propylene oxide (PO) is an essential feedstock in the plastic industry, as it is utilized in the production of chemicals and polymers.[1,2] According to forecasts, the yearly demand for PO is expected to surpass 20 Mt by 2025.[2] PO can be generated by the epoxidation of propylene. The three industrial techniques for PO production are the chlorohydrin process, organic hydroperoxide-based processes, and hydrogen peroxide (H_2O_2)-to-propylene oxide (HPPO) processes.[2–7] The chlorohydrin process is known to have significant environmental drawbacks

[a]Institute of Chemistry, Academia Sinica, Nankang, Taipei 115201, Taiwan, ROC. E-mail: sfyu@gate.sinica.edu.tw

[b]Department of Applied Chemistry, National Yang-Ming Chiao Tung University, Hsinchu 300093, Taiwan, ROC

[c]Sustainable Chemical Science and Technology (SCST), Taiwan International Graduate Program (TIGP), Academia Sinica, Nankang, Taipei 115201, Taiwan, ROC

[d]Department of Chemistry, National Tsing Hua University, Hsinchu 300044, Taiwan, ROC. E-mail: cmyang@mx.nthu.edu.tw

[e]College of Semiconductor Research, National Tsing Hua University, Hsinchu 300044, Taiwan, ROC

† Electronic supplementary information (ESI) available. See DOI: https://doi.org/10.1039/d4ta08256g

as it generates halogen and alkali salt wastes.[3,5] The processes based on organic hydroperoxides (*e.g.*, cumene hydroperoxide, *tert*-butyl hydroperoxide and ethylbenzene hydroperoxide) usually need additional purification steps to separate PO from co-products (*e.g.*, styrene and *tert*-butanol).[3,8] With the high reactivity of cumene with O_2, however, the Sumitomo process using Ti-containing silica catalysts can efficiently recycle cumene for PO production.[6] In comparison, the direct use of H_2O_2 for epoxidizing propylene with water as the only co-product is much more appealing from both environmental and economic points of view. The developed commercial HPPO plants produce H_2O_2 by the oxidation and reduction of anthraquinones or related molecules[9,10] and use titanosilicalite-1 (TS-1)[11,12] catalysts for the epoxidation reaction.[13–16] Alternatively, H_2O_2 can be generated *in situ* by gas-phase reactions of H_2 and O_2,[13] but temperature control is crucial for the gas-phase HPPO process because over-oxidation of PO may take place at high temperatures. In addition to the three industrial processes, direct epoxidation of propylene with O_2 over copper and silver-based catalysts has also been studied.[4,17] However, the reaction typically occurs at high temperatures, thermodynamically favoring C–H bond cleavage rather than double bond

This journal is © The Royal Society of Chemistry 2025

J. Mater. Chem. A, 2025, **13**, 5261–5274 | **5261**

epoxidation,[18] and therefore PO's selectivity and formation rate are typically low.[4]

Reports have shown that the reaction conditions and catalyst type greatly affect the selectivity of PO (S_{PO}), conversion of H_2O_2 ($X_{H_2O_2}$), and the utilization efficiency of H_2O_2 ($U_{H_2O_2}$) in the HPPO process. The reaction is typically carried out under mild conditions (around 40 °C and 1–10 bar) with protic (*e.g.*, methanol, water, and other alcohols) or aprotic (*e.g.*, acetonitrile and acetone) solvents.[19,20] For the reaction catalyzed by TS-1, Liu *et al.* compared the catalytic performance in methanol and acetonitrile. They found that lower PO selectivity (S_{PO} = 95%) and higher conversion of H_2O_2 ($X_{H_2O_2}$ = 97%) were obtained for the reaction conducted in methanol than that in acetonitrile (S_{PO} = 100% and $X_{H_2O_2}$ = 66%).[21] As a protic solvent, methanol may coordinate with the Ti centers and employ hydrogen bonding to stabilize a five-membered Ti-hydroperoxide (Ti–OOH) intermediate with high efficiency,[22,23] but solvolysis (or hydrolysis in the case of water) of PO may take place, lowering the PO selectivity.[6,24] In an aprotic solvent like acetonitrile, on the other hand, apart from the higher solubility of propylene than that in methanol, the Ti–OOH intermediate is not stabilized by hydrogen bonding,[25,26] but possible solvolysis of PO may be prevented.[27] Moreover, acetonitrile may react with H_2O_2 to form a peroxyacetimidic acid intermediate (CH$_3$–C(=NH)–O–O–H) to create an additional organic hydroperoxide-like route of epoxidation.[7,28,29] In addition, the coordination state of Ti species has been shown to influence the catalytic activity of TS-1 and related Ti-based catalysts for the HPPO reaction and epoxidation of other alkenes.[30–33] For example, Wang *et al.* prepared a TS-1 material with penta-coordinated (Ti(OH)$_2$(-OSi)$_3$) and hexa-coordinated (Ti(OH)$_4$(OSi)$_2$) Ti sites. They found that the hexa-coordinated Ti sites exhibit significantly higher catalytic activity than the penta- and tetra-coordinated sites in TS-1.[32] Other Ti-containing catalysts, including Ti-substituted BEA zeolites,[11,34] Ti-substituted MWW zeolites,[12,25] and even zeolites or oxide materials containing Nb, Ta or other metals,[35,36] have also been investigated for the HPPO reaction and alkene epoxidation.

Herein, we report the study on the HPPO reaction over zinc oxide (ZnO) with acetonitrile as a solvent. ZnO is a cheap, nontoxic material with unique physical and chemical properties and shows attractive applications in optoelectronics, electronics, laser technology, and photocatalysis.[37,38] It has been demonstrated that ZnO with a hexagonal wurtzite structure could interact with H_2O_2 and convert to cubic zinc peroxide (ZnO$_2$)[39] and that ZnO$_2$ may partially decompose to produce O$_2$ and hexagonal ZnO with a significant number of defects as the temperature increases, with a complete decomposition taking place at around ~250 °C.[39] ZnO$_2$ may react with water to produce paramagnetic superoxide species[40,41] and has been applied for reactions including the oxidation of aromatic alcohols to the corresponding carbonyl compounds,[42] decomposition of dye molecules in wastewater,[43] and detoxification of mustard gas.[44] As for the HPPO or related reactions, rather limited studies on ZnO-based catalysts, mainly in photocatalysis, *e.g.*, photocatalytic olefin epoxidation with O$_2$ over Pd/ZnO[45] and cyclohexane oxidation/epoxidation with H_2O_2 over

Fe$_2$O$_3$–ZnO[46] have been reported. It is noted that Arca and coworkers reported the preparation of zinc salt pre-treated TS-1 for the HPPO reaction[47] and found that the coordination of Zn to the Ti site (through bridging oxygen) resulted in the increase in the solvent donor properties to the Ti site as well as the reduction of the Ti–OOH electrophilicity, thereby giving rise to high S_{PO} and $U_{H_2O_2}$. However, the contribution from ZnO$_2$ possibly formed during the reaction was not discussed. In this study, ZnO nanorods (NRs; the sample is designated as ZnO-NR) and the composites of ZnO-NR and mesoporous MCM-41 materials (designated as ZnO/MCM-41) were prepared and applied to catalyze the reaction of propylene epoxidation with aqueous H_2O_2 in acetonitrile. As compared to ZnO-NR, ZnO/MCM-41 with optimum composition exhibited superior epoxidation performance with an S_{PO} of 100% and a $U_{H_2O_2}$ of over 98%. The fresh and spent catalysts of ZnO-NR and the best ZnO/MCM-41 composite, as well as the ZnO$_2$ nanoparticles (NPs), were characterized by multiple techniques, including synchrotron powder X-ray diffraction (SXRD), transmission electron microscopy (TEM), and X-ray absorption spectroscopy (XAS). Electron paramagnetic resonance (EPR) spectroscopy and X-ray photoelectron spectroscopy (XPS) were applied to investigate the possible reactive species formed in the working catalysts. Based on the results, a possible reaction mechanism of the HPPO process over ZnO/ZnO$_2$ catalysts was proposed.

2 Materials and methods

2.1. Chemicals and materials

All chemicals, including zinc acetate dihydrate (Zn(CH$_3$COO)$_2$·2H$_2$O, 99.8%), zinc nitrate hexahydrate (Zn(NO$_3$)$_2$·6H$_2$O, 98%), ethanol (EtOH, 99.9%), sodium hydroxide pellets (NaOH, 99.9%), hydrogen peroxide (H_2O_2, 35 wt% aqueous solution), and acetonitrile (CH$_3$CN, 98%), were of analytical grade purchased from Sigma-Aldrich and were used without further purification. The propylene oxide standard (C$_3$H$_6$O, 99%) and methanol (CH$_3$OH, 99%) were purchased from Sigma-Aldrich, whereas 7 N ammonia (NH$_3$) solution was purchased from Acros Organics. The propylene gas was purchased from Huei Chyi Gas Co. Ltd, Taiwan. The mesoporous MCM-41 material (CAS no. 1318-02-1) was also purchased from Sigma-Aldrich. Isotope-labeled H$_2$^{18}O$_2$ (90 atom%, 2.0–2.4% aqueous solution) and ^{18}O$_2$ (97 atom%) were purchased from ICON Isotopes and Sigma-Aldrich, respectively.

2.2. Catalyst preparation

The ZnO-NR sample was prepared by a reported solvothermal method.[48] Zn(CH$_3$COO)$_2$·2H$_2$O (2.195 g) and NaOH (0.8 g) were first dissolved in ethanol (80 mL). The solution was poured into a 15 mL Teflon-sealed autoclave and was heated at 180 °C for 12 h. The solid product was collected by centrifugation and was repeatedly washed with ethanol and water. The dried solid was further heated at 500 °C for 3 h with a temperature ramp of 10 °C min^{-1}. The composites of ZnO-NR and MCM-41 were prepared by the immobilization method.[49,50] A total of 25 mg of ZnO-NR was added into 75 mg of MCM-41 and stirred in

5262 | *J. Mater. Chem. A*, 2025, **13**, 5261–5274

This journal is © The Royal Society of Chemistry 2025

a mixture of CH_3CN (40 mL) and 10 mL of EtOH (4/1 v/v) at 30 °C, and 7 N ammonia solution in methanol (2 mL) was added dropwise into the mixture to reach a pH value of 9.0. After the mixture was further stirred for 12 h, the solid was collected by centrifugation, washed with ethanol, and dried at 60 °C in a vacuum. The composites are designated as ZnO/MCM-41(x), where x denotes the content of Zn in the composites (wt%; x = 0.82–9.41). A reference sample of ZnO_2 NPs was also prepared by mixing an aqueous solution of $Zn(CH_3COO)_2 \cdot 2H_2O$ (1.0 g in 50 mL of water) with an aqueous solution of H_2O_2 (35 wt%, 2 mL).[51] The mixture was stirred at room temperature for 12 h, and the solid product of ZnO_2 NPs was collected by centrifugation, washed with water, and dried at 60 °C under vacuum.

2.3. Catalyst characterization

SXRD patterns were recorded using the TPS 19A1 beamline, with an X-ray wavelength of 0.77489 Å, at the National Synchrotron Radiation Research Center (NSRRC), Taiwan. TEM images were obtained using a JEOL JEM-F200 microscope operating at 200 kV. The compositions of the ZnO-based materials were determined using an inductively coupled plasma-mass spectrometer (ICP-MS, Thermo-element XR) and energy dispersive X-ray spectroscopy (EDX) on a field-emission scanning electron microscope (SEM, FEI Quanta 200F) with an EDX detector (ULTRA PLUS, Carl Zeiss). The SEM images were obtained using the microscope operated at 10 kV. Nitrogen physisorption isotherms were obtained at 77 K using a Micromeritics 3Flex instrument. Each sample was evacuated at 120 °C for 12 h prior to the measurement. The Brunauer–Emmett–Teller (BET) surface area was calculated from the adsorption branch in the relative pressure range of 0.05–0.30, and the average pore diameter was calculated from the desorption branch using the Barrett–Joyner–Halenda (BJH) method. The total pore volume was evaluated at a relative pressure of 0.95. XAS measurements at the Zn K-edge were conducted in transmission mode using the TLS 17C1 and TPS 44A beamlines at the NSRRC, Taiwan. Zinc foil was measured simultaneously as a reference sample for energy calibration. Multiple scans were performed and averaged to enhance the signal-to-noise ratio. For a measured spectrum, the extended X-ray absorption fine structure (EXAFS) function χ was obtained by subtracting the post-edge background from the initial spectrum and then normalizing to the edge jump step. The energy space spectrum of the normalized $\chi(E)$ was then transformed into the k-space spectrum of $\chi(k)$. The $\chi(k)$ was multiplied by k^3 to compensate for the oscillation dampening in the high-k region, and the k^3-weighted EXAFS data in the range of 3.0–14 Å^{-1} were converted to the R-space data by Fourier transform (FT). Athena software was used to process the XAS spectra, including background subtraction, normalization of the edge jump step, and FT of the k^3-weighted EXAFS data. Artemis software was used to fit the FT profiles. Wavelet transform analysis was further conducted to gain more insights into the k-space resolution. Athena software was also used for linear combination fitting (LCF) of XANES and k^3-weighted EXAFS data of the spent catalysts. EPR spectra were recorded on a Bruker EMX spectrometer (Bruker ST4102 cavity)

operating at X-band frequency and 100 kHz field modulation. To insert the sample (10 mg), a cylindrical quartz tube container was used, which was maintained at a temperature of 77 K. Thermogravimetric analysis combined with gas chromatography and mass spectrometry (TGA-GC/MS) was conducted on a Mettler-Toledo 2-HT analyzer coupled with an Agilent 7890 GC/5975 MS system. XPS measurements were performed on an ultrahigh vacuum system using an Omicron DAR400 Al Kα X-ray source and an Omicron EA125 energy analyzer. The C 1s core level peak (284.8 eV) was used as an energy reference, and the XPS spectra were analyzed using CasaXPS software.

2.4. Epoxidation of propylene with hydrogen peroxide

The catalytic HPPO reactions were carried out in a 50 mL stainless steel Parr autoclave reactor equipped with a Teflon liner. The autoclave was loaded with a catalyst (12.5–62.5 mg), H_2O_2 (35 wt% aqueous solution, 5.87–14.10 mmol), and CH_3CN (5 mL). The reactor was sealed, pressurized with propylene (5–20 bar), and then heated to the designated temperature (30–70 °C). The reaction mixture was stirred at 880 rpm and allowed to react for 1–8 h (starting from the time when the reaction mixture reached the designated temperature). After the reaction was complete, the stirring was stopped, and to avoid loss of PO (with a boiling point of ~35 °C), the reactor was cooled to 10 °C using iced water before being slowly depressurized and opened. The reaction products were analyzed by gas chromatography (GC, Shimadzu GC-2010plus) or GC/MS (Agilent GC/MS-5977B/MSD) with methyl *tert*-butyl ether (MTBE) as an internal standard. The amount of H_2O_2 remaining after the reaction was determined by UV-vis spectroscopy with a potassium titanium oxalate solution.[52,53] For the catalytic test of ethylene epoxidation, the products were analyzed by ^{1}H-NMR on a Bruker AVA-AV400 (400 MHz) spectrometer. All resonances were referenced to the deuterated solvent CD_3CN (δ = 1.93 ppm). The ZnO-NR and ZnO/MCM-41(7.99) catalysts after the catalytic tests under optimum reaction conditions were collected by centrifugation for further characterization, and the spent catalysts are designated by adding "sp" to the designation of the original catalysts (*e.g.*, ZnO-NR$_{sp}$ refers to the ZnO-NR collected after the catalytic reaction). Small losses of the spent catalyst during collection by centrifugation were accounted for to keep the mass of the applied catalyst constant in the recyclability test. The values of conversion of H_2O_2 ($X_{H_2O_2}$), the utilization efficiency of H_2O_2 ($U_{H_2O_2}$), the yield of PO (Y_{PO}, based on the initial molar amount of H_2O_2), the selectivity of PO (S_{PO}), the productivity of PO (P_{PO}), and the turnover number (TON) were calculated using these criteria:

$$X_{H_2O_2} (\%) = \frac{n^0_{H_2O_2} - n_{H_2O_2}}{n^0_{H_2O_2}} \times 100\% \tag{1}$$

$$U_{H_2O_2}(\%) = \frac{n_{PO}}{n^0_{H_2O_2} - n_{H_2O_2}} \times 100\% \tag{2}$$

$$Y_{PO} (\%) = \frac{n_{PO}}{n^0_{H_2O_2}} \times 100\% \tag{3}$$

This journal is © The Royal Society of Chemistry 2025

J. Mater. Chem. A, 2025, **13**, 5261–5274 | **5263**

$$S_{PO}(\%) = \frac{n_{PO}}{n_{PO} + n_{others}} \times 100\% \qquad (4)$$

$$P_{PO}(\text{mg h}^{-1}\, g_{cat}^{-1}) = \frac{w_{PO}}{time \times w_{cat}} \qquad (5)$$

$$TON = \frac{n_{PO} + n_{others}}{n_{Zn}} \qquad (6)$$

where $n_{H_2O_2}^0$ and $n_{H_2O_2}$ denote the molar amounts of H_2O_2 before and after the reactions, n_{PO} denotes the molar amount of PO formed (calculated from the volume of the reaction mixture and the value of molar concentration determined by GC or GC/MS), n_{others} denotes the molar amount of other byproducts detected, w_{PO} and w_{cat} denote the weights of PO formed and the catalyst and n_{Zn} denotes the molar amount of Zn in a catalyst. Some catalysts also produced acetic acid (AC) or acetaldehyde (AA), and the criteria for the yields and selectivity of these reaction products were the same as those for PO.

3   Results and discussion

3.1.   Catalytic study of propylene epoxidation

The structure and morphology of all the ZnO-NR and ZnO/MCM-41(x) materials were well characterized by SXRD, TEM, and SEM. The compositions of the ZnO/MCM-41(x) composites were determined by ICP-MS and EDX. The catalytic performance of ZnO-NR for propylene epoxidation with H_2O_2 in CH_3CN was first examined with varied amounts of H_2O_2 (Entries 1–5, Table 1). While no PO was produced in the absence of H_2O_2 (Entry 1, Table 1), efficient conversion of propylene to PO with nearly 100% selectivity was observed in the presence of H_2O_2 and ZnO-NR. With an amount of 5.87 mmol H_2O_2 for a reaction of 6 h, the conversion of H_2O_2 ($X_{H_2O_2}$) and the utilization efficiency of H_2O_2 ($U_{H_2O_2}$) reached 97.98% and 97.53%, respectively. Under the reaction conditions, the yield of PO (Y_{PO}) based on the initial molar amount of H_2O_2 reached 95.56% and the productivity of PO (P_{PO}) was 1448 mg h^{-1} g$_{cat}^{-1}$. The value of TON based on the molar amount of Zn was 14.3. As the amount of H_2O_2 increased up to 14.10 mmol, the reactions gave a higher TON and P_{PO} (23.3 and 2398 mg h^{-1} g$_{cat}^{-1}$ with 14.10 mmol H_2O_2, Table 1), but at the cost of reduced conversion and utilization efficiency of H_2O_2. The amount of 5.87 mmol H_2O_2 with the highest values of $X_{H_2O_2}$, $U_{H_2O_2}$, and Y_{PO} was thus chosen

to study other reaction parameters. Next, catalytic reactions with varied amounts (12.5–62.5 mg) of ZnO-NR were conducted (Entries 2, 6–9, Table 1). Basically, volcano relationships were observed between the amount of ZnO-NR, with an optimum value of 37.5 mg, and the parameters of $X_{H_2O_2}$, $U_{H_2O_2}$, and Y_{PO}. No PO was formed in the blank test with no ZnO-NR. It was noted that acetic acid (AC) as an over-oxidized minor product was detected with smaller (12.5 and 25.0 mg) amounts of ZnO-NR, and an AC selectivity of 10.41% was measured with 12.5 mg of ZnO-NR. Finally, the choice of solvent was examined and the mixtures of acetonitrile and water, water, and methanol were applied to the reaction. Under conditions similar to those for Entry 2 of Table 1 (5.87 mmol of H_2O_2, 37.5 mg of a catalyst, 5 mL of solvent, and 20 bar propylene pressure at 50 °C for 6 h), we found worse catalytic performance of ZnO-NR in the acetonitrile/water mixtures than in pure acetonitrile and observed no conversion of propylene in water or methanol (Table S1†). The results clearly demonstrated the crucial role of acetonitrile as a solvent in the catalytic reaction over ZnO-based catalysts.

Since ZnO-NR contained aggregates of nanorods and exhibited a relatively low surface area (31 m^2 g^{-1}, $cf.$ Fig. S1 and Table S2†), an attempt was made to disperse and immobilize varied amounts of ZnO-NR on mesoporous MCM-41 aluminosilicate (with a BET surface area of 856 m^2 g^{-1} and an average pore diameter of 3.1 nm, $cf.$ Fig. S1 and Table S2†) for the catalytic reaction. We first examined the catalytic performance of the composite catalysts ZnO/MCM-41(x) with varying Zn content x (in wt%) (Table 2). While MCM-41 alone did not exhibit any catalytic activity, the composites with a Zn content higher than 1.45% were capable of epoxidizing propylene (Table 2). Except for ZnO/MCM-41(1.45), for which acetaldehyde (AA) appeared as the major product, other composite catalysts with higher Zn contents showed 100% selectivity of PO. The values of $X_{H_2O_2}$ and $U_{H_2O_2}$, as well as Y_{PO}, increased with increasing the Zn content of the composites. The best catalyst among the composites prepared and studied was ZnO/MCM-41(7.99), showing nearly 100% PO selectivity (S_{PO}), H_2O_2 utilization efficiency ($U_{H_2O_2}$ = 98.33%) and PO yield (Y_{PO} = 97.44%) under the reaction conditions at 50 °C for 6 h. The catalytic performance of ZnO/MCM-41(7.99) (Entry 7, Table 2) and ZnO-NR under otherwise the same reaction conditions (Entry 2, Table 1) was

Table 1   Results of propylene epoxidation over ZnO-NR with H_2O_2 using varied amounts of ZnO-NR and H_2O_2[a]

No	ZnO-NR (mg)	H_2O_2 (mmol)	$X_{H_2O_2}$ (%)	$U_{H_2O_2}$ (%)	Y_{PO} (%)	S_{PO} (%)	P_{PO} (mg h^{-1} g$_{cat}^{-1}$)	Y_{AC} (%)	S_{AC} (%)	TON
1	37.5	0	0	0	0	ND[b]	0	—	—	0
2	37.5	5.87	97.98	97.53	95.56	100	1448	—	—	14.3
3	37.5	9.34	74.43	85.82	64.11	100	1546	—	—	15.1
4	37.5	11.75	74.70	85.26	63.69	100	1932	—	—	18.8
5	37.5	14.10	77.19	85.33	65.87	100	2398	—	—	23.3
6	12.5	5.87	72.07	48.04	34.62	89.59	1574	4.02	10.41	15.3
7	25.0	5.87	86.71	75.91	65.82	97.23	1496	1.88	2.77	14.6
8	50.0	5.87	86.39	93.61	80.87	100	919	—	—	9.0
9	62.5	5.87	88.95	96.28	85.64	100	779	—	—	9.0

[a] Reactions were conducted with 5 mL of CH_3CN and a propylene pressure of 20 bar at 50 °C for 6 h. [b] Not determined.

Table 2 Results of propylene epoxidation over ZnO/MCM-41(x) with H_2O_2 using varying Zn loadings[a]

No	Zn content x (wt%)	$X_{H_2O_2}$ (%)	$U_{H_2O_2}$ (%)	Y_{PO} (%)	S_{PO} (%)	P_{PO} (mg h^{-1} g$_{cat}^{-1}$)	Y_{AA} (%)	S_{AA} (%)	TON
1	0	ND[b]	ND	0	ND	0	—	—	0
2	0.82	ND	ND	0	ND	0	—	—	0
3	1.45	10.36	24.52	2.54	15.84	39	5.12	84.16	20.5
4	4.23	44.06	80.79	35.60	100	538	—	—	90.7
5	4.34	49.91	80.54	40.20	100	609	—	—	94.5
6	4.83	60.83	94.38	57.41	100	871	—	—	120.5
7	7.99	99.09	98.33	97.44	100	1476	—	—	124.4
8	9.41	95.46	97.35	92.93	100	1408	—	—	101.0

[a] Reactions were conducted with 5.87 mmol of H_2O_2, 37.5 mg of catalyst, 5 mL of solvent, and a propylene pressure of 20 bar at 50 °C for 6 h. [b] Not determined.

compared. With the same catalyst amount of 37.5 mg, the Zn (or ZnO) content in ZnO/MCM-41(7.99) was much lower than that for ZnO-NR. The fact that both catalysts produced PO as the only product and exhibited similar or comparable values of $X_{H_2O_2}$, $U_{H_2O_2}$, Y_{PO}, and P_{PO} clearly indicated that ZnO-NR was successfully dispersed and immobilized on MCM-41 to expose a larger catalytically active surface area to convert propylene to PO with H_2O_2 in acetonitrile. As a result of low Zn (or ZnO) content, the calculated value of TON for ZnO/MCM-41(7.99) (124.4) was nearly an order of magnitude higher than that for ZnO-NR (14.3). The reactions with varied amounts of H_2O_2 and ZnO/MCM-41(7.99) were further conducted (cf. Table S3†). In these reactions (except the one without adding H_2O_2), PO was the only product (i.e., S_{PO} = 100%) and acetic acid was not detected. Similar to the trends observed for ZnO-NR, an increase in the amount of H_2O_2 resulted in lower values of H_2O_2 conversion, H_2O_2 utilization efficiency, and PO yield but better TON and PO productivity. The highest values of TON (225.0) and P_{PO} (2691 mg h^{-1} g$_{cat}^{-1}$) were observed for the reaction with 14.1 mmol H_2O_2. Besides, similar volcano relationships between the catalyst amount and parameters of $X_{H_2O_2}$, $U_{H_2O_2}$, and Y_{PO} were also observed for ZnO/MCM-41(7.99).

The influences of propylene pressure and reaction temperature on the catalytic performance of ZnO-NR and ZnO/MCM-41(7.99) with fixed amounts of catalyst (37.5 mg), H_2O_2 (5.87 mmol), and acetonitrile (5 mL) were then studied. The results of the reactions with propylene pressures of 5–20 bar at 50 °C for 6 h are shown in Fig. 1a and Tables S4 and S5.† For both catalysts, PO was the only detected product, and the conversion and utilization efficiency of H_2O_2, the yield of PO, and TON all increased with increasing propylene pressure. The results suggest that the mass transfer of the gaseous reactant is a limiting factor for the catalytic process. Next, catalytic reactions with a propylene pressure of 20 bar over the two catalysts at 30–70 °C were conducted for 6 h. As shown in Fig. 1b and Tables S4 and S5,† while all the reactions exhibited 100% selectivity for PO, volcano relationships were observed between the reaction temperature and $X_{H_2O_2}$, $U_{H_2O_2}$, Y_{PO}, and TON for both ZnO-NR and ZnO/MCM-41(7.99). The poorer catalytic performance at a temperature higher than 50 °C may be attributed to the accelerated decomposition of H_2O_2.[54]
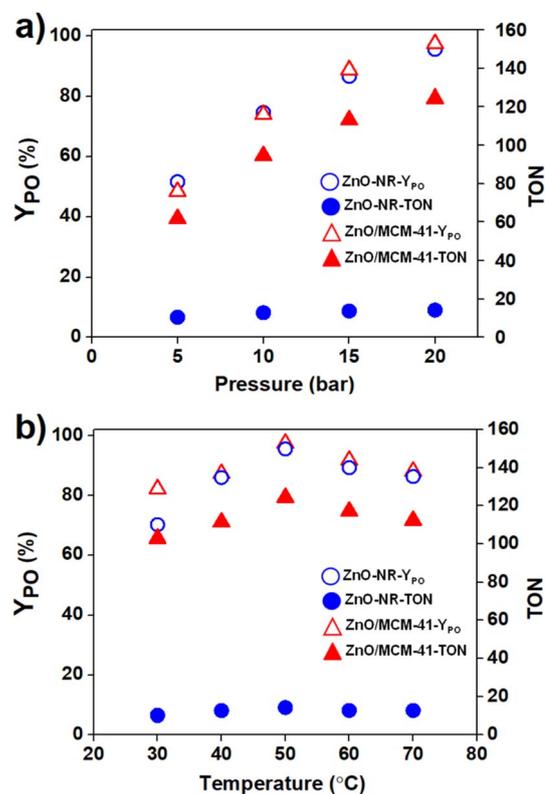

Fig. 1 Effects of (a) propylene pressure (at 50 °C) and (b) reaction temperature (with 20 bar propylene pressure) on PO yield (Y_{PO}) and TON for the reactions over ZnO-NR and ZnO/MCM-41(7.99) with fixed amounts of H_2O_2 (5.87 mmol), catalyst (37.5 mg), and acetonitrile (5 mL) for 6 h.

Changes in catalytic performance with time for the reactions over ZnO-NR and ZnO/MCM-41(7.99) were then compared. As shown in Fig. 2a, for both catalysts, no induction time was observed for the catalytic reactions to start, and the evolutions of H_2O_2 conversion and PO yield are very close to each other, implying a one-to-one equivalence of the limiting reactant H_2O_2 and the produced PO. The values of $X_{H_2O_2}$ and Y_{PO} (and $U_{H_2O_2}$, Table S6†) for the two catalysts are similar, which should be, as aforementioned, associated with the dispersion of ZnO-NR on MCM-41. The 6 h and 8 h TON values are very close (Table S6†),
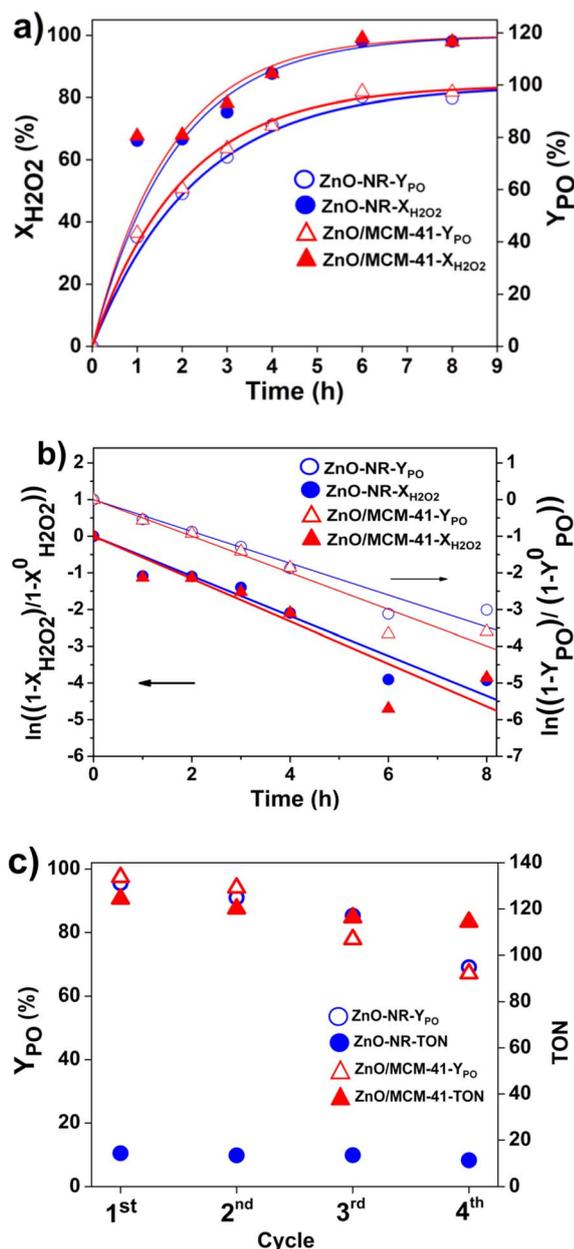
This journal is © The Royal Society of Chemistry 2025

J. Mater. Chem. A, 2025, 13, 5261–5274 | **5265**

Fig. 2 (a) Changes in H_2O_2 conversion ($X_{H_2O_2}$) and PO yield (Y_{PO}) with reaction time for propylene epoxidation over ZnO-NR and ZnO/MCM-41(7.99) with 5.87 mmol of H_2O_2, 37.5 mg of catalyst, 5 mL of CH_3CN, and a propylene pressure of 20 bar at 50 °C. (b) Time courses fitted with the pseudo-first-order kinetic model. (c) Y_{PO} and TON for the two catalysts in cycle tests of propylene epoxidation with 5.87 mmol of H_2O_2, 37.5 mg of catalyst, 5 mL of CH_3CN, and a propylene pressure of 20 bar at 50 °C for 6 h.

indicating that the reactions over the two catalysts approached completion within 6 h. The time courses shown in Fig. 2a and b could be well fitted with the pseudo-first-order kinetic model, and the derived rate constants (k) from PO yield are 0.43 h^{-1} for ZnO-NR (with a correlation coefficient (R^2) of 0.941) and 0.50 h^{-1} for ZnO/MCM-41(7.99) ($R^2 = 0.948$). Poorer fittings were found for the data of H_2O_2 conversion, and the rate constant values derived from H_2O_2 conversion are slightly higher than

those derived from Y_{PO} ($k = 0.54$ h^{-1} and $R^2 = 0.929$ for ZnO-NR; $k = 0.58$ h^{-1} and $R^2 = 0.875$ for ZnO/MCM-41(7.99)). This may be attributed to the spontaneous decomposition of H_2O_2 under the reaction conditions.

The stability of ZnO-NR and ZnO/MCM-41(7.99) was further examined. After the reactions with 5.87 mmol of H_2O_2, 37.5 mg of catalyst, 5 mL of CH_3CN, and a propylene pressure of 20 bar at 50 °C for 6 h, the spent catalysts were collected and reused to catalyze the reactions under the same conditions for four cycles. The results of cycle tests are shown in Fig. 2c and Table S7.† Slight decreases in $X_{H_2O_2}$, $U_{H_2O_2}$, Y_{PO}, P_{PO}, and TON were found for both catalysts, and around a 10% drop in TON was observed after the fourth cycle. The decreases may be mainly associated with the loss of catalysts during the collection of spent catalysts by centrifugation. For ZnO/MCM-41(7.99), a slight degree of leaching of Zn species was another reason, and a Zn leaching of ~5.7% was detected by ICP-MS after the fourth cycle. With factors of catalyst loss and Zn leaching being taken into account, the calculated values of TON and other parameters are very close to those for the first catalytic cycle, suggesting high stability of the catalysts. A comparison of the catalytic performance of ZnO-NR and ZnO/MCM-41(7.99) with reported HPPO catalysts was made. As shown in Table S8,† the values of PO yield, PO selectivity, H_2O_2 conversion, and H_2O_2 utilization for ZnO-NR and ZnO/MCM-41(7.99) are comparable to those for industrially applicable TS-1 catalysts[25,55] for the epoxidation of propylene with $H_2O_{2(aq)}$. The two ZnO-based catalysts outperform the Nb-EISA catalyst[35,36] in terms of PO yield and H_2O_2 conversion.

An attempt was made to test the catalytic activity of the best catalyst, ZnO/MCM-41(7.99), for the epoxidation of ethylene. The reaction was conducted with 2.94 mmol of H_2O_2, 37.5 mg of catalyst, 2.5 mL of deuterated acetonitrile (CD_3CN), and an ethylene pressure of 20 bar at 50 °C for 6 h, and the solution collected after the reaction by centrifugation was analyzed by ^{1}H-NMR. Ethylene oxide (EO), identified by the signal at 2.64 ppm (Fig. S2†), was the major product of the reaction with a selectivity of 92.73%, with ethylene glycol as the only minor product. The conversion and utilization of H_2O_2 were lower than the values for the reaction of propylene epoxidation (Table S9†), despite a lower initial amount of the oxidant. Nevertheless, the results show that ZnO/MCM-41(7.99) could catalyze the epoxidation of ethylene, giving an EO yield of 67.26%, an EO productivity of 387 mg h^{-1} g$_{cat}$$^{-1}$, and a TON of 46.3 under the reaction conditions.

3.2. Structural analysis of fresh and spent catalysts

The synchrotron powder X-ray diffraction (SXRD) patterns (X-ray wavelength of 0.77489 Å) of ZnO-NR and ZnO/MCM-41(x) all showed sharp peaks at 15.96°, 17.15°, 18.16°, 23.52°, 27.87°, and 30.53° (Fig. 3 and S3†), which correspond to the (100), (002), (101), (102), (210), and (103) reflections of crystalline ZnO with a hexagonal wurtzite structure (space group: $P6_3mc$; lattice constants: $c = 5.21$ Å and $a = 3.25$ Å).[56] For ZnO/MCM-41(x), the peaks in the small-angle region correspond well to the reflections of MCM-41 exhibiting a two-dimensional hexagonal
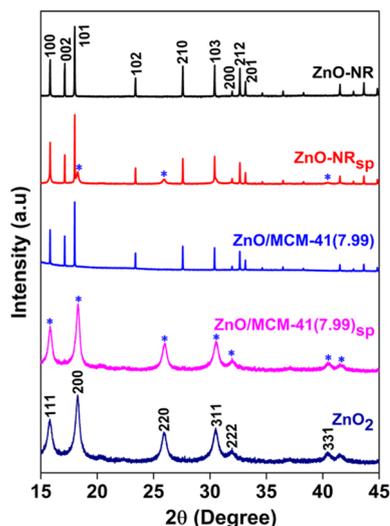
5266 | J. Mater. Chem. A, 2025, 13, 5261–5274

This journal is © The Royal Society of Chemistry 2025

Fig. 3 SXRD patterns of ZnO-NR, ZnO-NR$_{sp}$, ZnO/MCM-41(7.99), ZnO/MCM-41(7.99)$_{sp}$, and ZnO$_2$ NPs (X-ray wavelength of 0.77489 Å). The peaks marked by asterisks are attributed to cubic ZnO$_2$.

mesostructure (with a unit cell parameter of ~3.9 nm).[57] The nanorod morphology of ZnO was confirmed by SEM (Fig. S4†). The nanorods in ZnO-NR were mostly assembled or bundled, while those in ZnO/MCM-41(x) were mainly segregated, presumably by the mixed MCM-41 particles. The MCM-41 particles could be observed in the samples with a relatively higher amount of the material (e.g. ZnO/MCM-41(4.23), Fig. S4e†), but they could not be clearly discerned in ZnO/MCM-41(7.99) due to the low contrast and low relative amount of MCM-41. The SEM observation confirmed the role of MCM-41 in dispersing ZnO nanorods to expose the surface of segregated nanorods for catalysis. TEM was further performed to analyze ZnO-NR and ZnO/MCM-41(7.99). For ZnO-NR, the bundled nanorods were again found (Fig. 4a), and fringe patterns were clearly observed in the ZnO nanorods in the high-resolution TEM (HRTEM) images (Fig. 4b). In ZnO/MCM-41(7.99), on the other hand, individual ZnO nanorods with high crystallinity were observed among irregularly shaped MCM-41 particles (Fig. 5a and b). Basically, the results of TEM are consistent with the SEM observations.

The ZnO-NR and ZnO/MCM-41(7.99) catalysts after the catalytic reactions under optimum conditions (i.e., 5.87 mmol of H$_2$O$_2$, 37.5 mg of catalyst, 5 mL of CH$_3$CN, and a propylene pressure of 20 bar at 50 °C for 6 h) were collected by centrifugation, and the spent catalysts ZnO-NR$_{sp}$ and ZnO/MCM-41(7.99)$_{sp}$ were further characterized in order to identify the active species for the reaction. ZnO-NR$_{sp}$ gave an SXRD pattern with some broad and weak reflections, in addition to those attributed to hexagonal ZnO (Fig. 3), suggesting the presence of some minor phase with relatively low crystallinity in the spent catalyst. For ZnO/MCM-41(7.99)$_{sp}$, the SXRD pattern is completely different from that of ZnO/MCM-41(7.99) and contains relatively broad reflections that could be indexed to
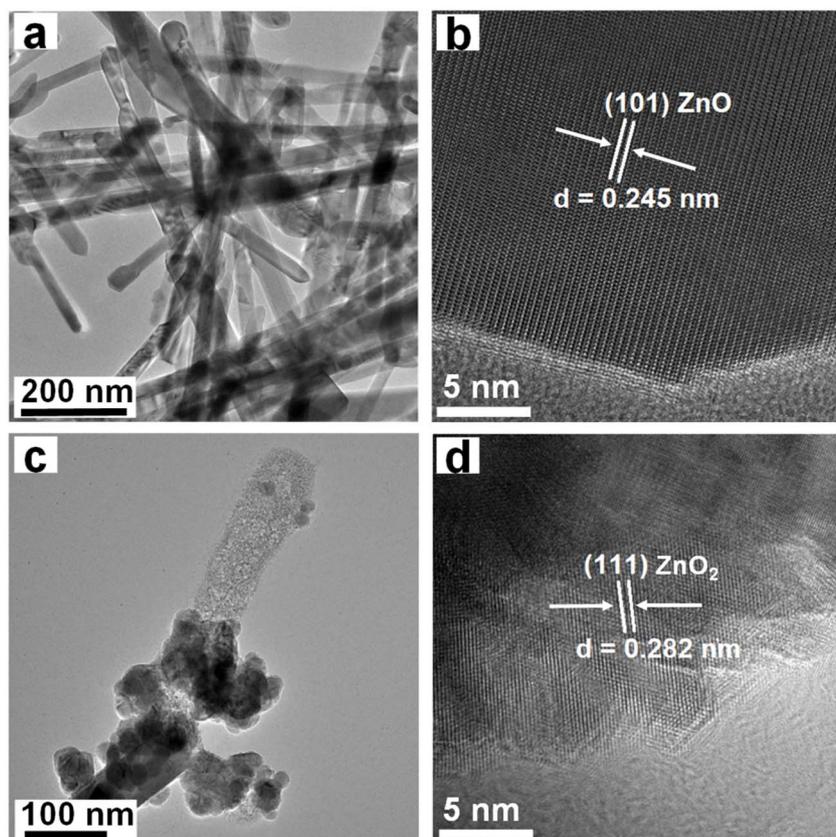

Fig. 4 TEM (a and c) and HRTEM (b and d) images of ZnO-NR (a and b) and ZnO-NR$_{sp}$ (c and d).
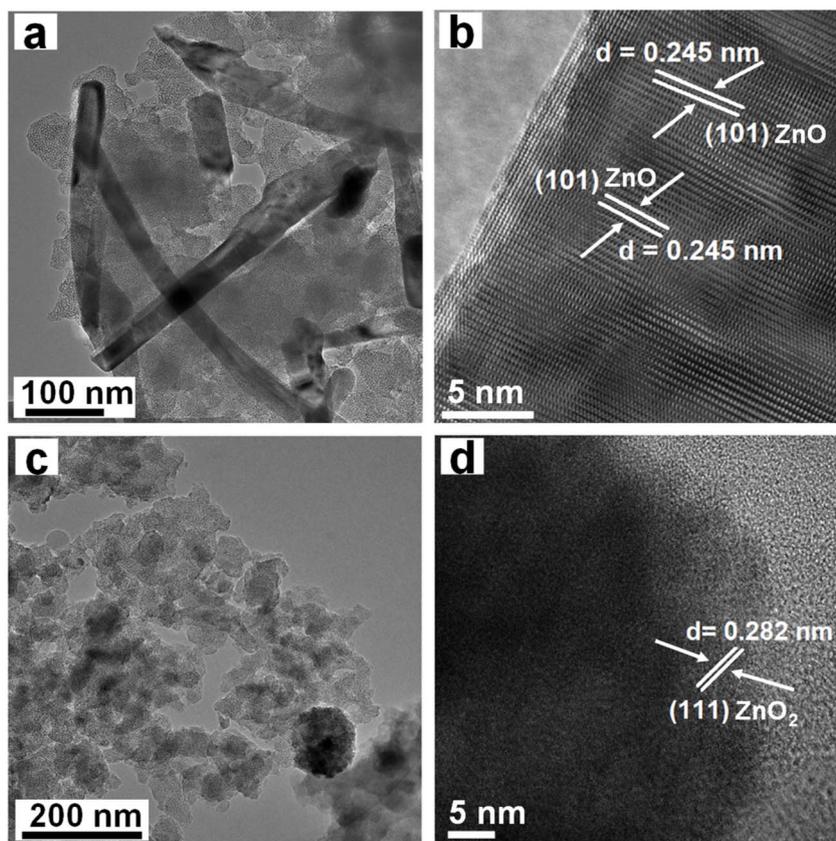
Fig. 5 TEM (a and c) and HRTEM (b and d) images of ZnO/MCM-41(7.99) (a and b) and ZnO/MCM-41(7.99)$_{sp}$ (c and d).

ZnO_2 with a cubic-pyrite structure (space group: $Pa\bar{3}$ lattice constants: $a = 4.87$ Å).[39] A reference sample of phase-pure cubic ZnO_2 NPs was synthesized by following a reported procedure.[51] Its SXRD pattern is also shown in Fig. 3, and analyses of TEM, HRTEM, and EDX revealed that the sample comprised particles with tens of nanometers in size, each of which contained nanosized domains of cubic ZnO_2 (Fig. S5†). Based on SXRD, the minor phase in ZnO-NR$_{sp}$ was identified to be ZnO_2 and the three additional peaks were indexed to be the (200), (220), and (331) reflections of cubic ZnO_2. The spent catalysts were further analyzed by TEM. Most ZnO nanorods in ZnO-NR$_{sp}$ were much shorter than those in the as-prepared catalyst, and some nanoparticles with irregular shapes (several to tens of nanometers in size) were also observed (Fig. 4c). The nanoparticles showed a lattice fringe spacing of 0.282 nm, corresponding to the (111) plane of cubic ZnO_2 (Fig. 4d). For ZnO/MCM-41(7.99)$_{sp}$, no rod-shaped particles were observed (Fig. 5c). EDX elemental mapping images confirmed that the Zn-containing species were dispersed in the composite (Fig. S6†), and the particles with darker contrast also showed lattice fringes of ZnO_2 (Fig. 5d). The results of SXRD and TEM/EDX indicated that ZnO nanorods interacted with H_2O_2 and converted to ZnO_2 NPs during the catalytic reaction. Moreover, while only part of the ZnO nanorods in ZnO-NR were converted, most ZnO nanorods in ZnO/MCM-41(7.99) were transformed into ZnO_2. Such a dramatic transformation may be attributed to the much better accessibility of the dispersed ZnO nanorods in the catalyst.

XAS measurements at the Zn K-edge were further conducted for bulk and quantitative analysis of the catalysts. ZnO-NR and ZnO/MCM-41(7.99) exhibited identical absorption edges (9661.30 eV) in their XANES spectra, while the edge for ZnO_2 NPs is slightly blue shifted to 9664.70 eV (Fig. 6a and b). The measured values of the absorption edge for the samples are almost identical to the reported values of bulk hexagonal ZnO[58] and cubic ZnO_2.[39] The slight difference in absorption edges for ZnO and ZnO_2 may be associated with the coordination geometry of Zn^{2+} in the two structures (four-coordinated tetrahedral geometry in hexagonal ZnO and six-coordinated octahedral geometry in cubic ZnO_2)[58,59] and the oxidation state of the coordinating oxygen anions. Moreover, the normalized white line absorption of ZnO-NR$_{sp}$ is more intense than that of ZnO-NR, possibly also associated with the change in the coordination state of Zn.[59] The fitted results of Zn K-edge k^3-weighted EXAFS data and their FT profiles as well as the wavelet transforms for EXAFS signals further confirmed the crystalline structure of hexagonal ZnO and cubic ZnO_2 in the samples (Table S10 and Fig. S7†). Next, the spent catalysts were analyzed. The absorption edges for ZnO-NR$_{sp}$ and ZnO/MCM-41(7.99)$_{sp}$ were in between those for ZnO-NR and ZnO_2 NPs (Fig. 6a and b), suggesting that the spent catalysts contained both ZnO and ZnO_2. The XANES spectra were fitted with those of ZnO-NR and ZnO_2 NPs by linear combination, and the results of LCF (Fig. 6c and d) suggested that around 50% (R factor = 0.001) and 77% (R factor = 0.003) of ZnO in ZnO-NR$_{sp}$ and ZnO/MCM-41(7.99)$_{sp}$,
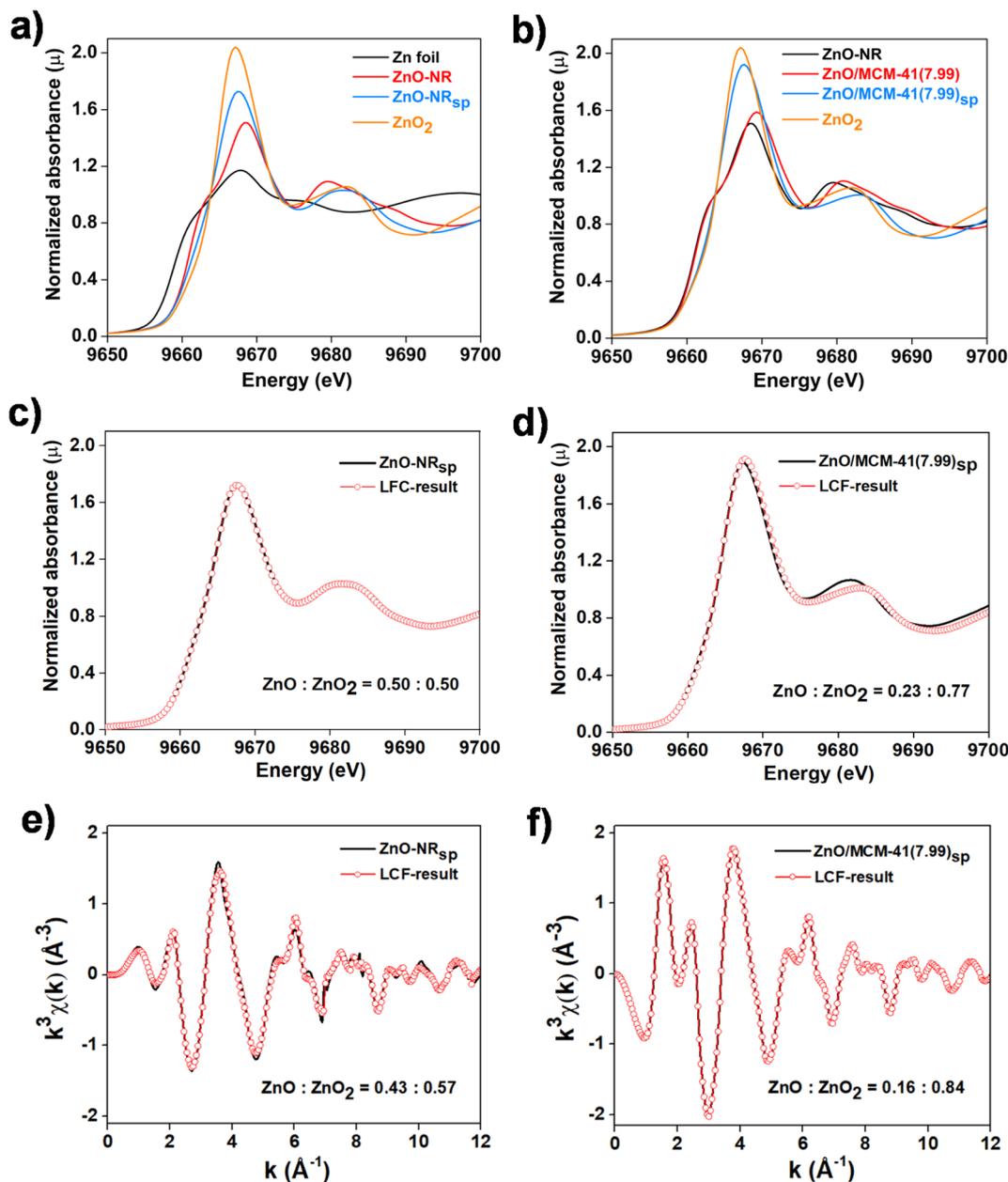
5268 | J. Mater. Chem. A, 2025, 13, 5261–5274

This journal is © The Royal Society of Chemistry 2025

Fig. 6 (a and b) Normalized Zn K-edge XANES spectra of Zn foil, ZnO-NR, ZnO-NR$_{sp}$, ZnO/MCM-41(7.99), ZnO/MCM-41(7.99)$_{sp}$, and ZnO$_2$ NPs. (c and d) LCF results for the Zn K-edge XANES of the spent catalysts. (e and f) LCF results for the k^3-weighted EXAFS data of the spent catalysts.

respectively, were converted to ZnO$_2$. The relative amounts of ZnO$_2$ in spent catalysts were also estimated by fitting the k^3-weighted EXAFS data (Fig. 6e and f), and the values of 57% (R factor = 0.034) for ZnO-NR$_{sp}$ and 84% (R factor = 0.034) for ZnO/MCM-41(7.99)$_{sp}$ were obtained. The quantitative analysis confirmed a higher degree of conversion of ZnO nanorods in ZnO/MCM-41(7.99) during the catalytic reaction than those in the ZnO-NR catalyst.

3.3. Study on active sites and the mechanism of the HPPO process over ZnO-based catalysts

The fact that a significant amount of ZnO converted to ZnO$_2$ during a catalytic reaction points to the possibility that ZnO$_2$ might

be the actual active species for the epoxidation of propylene. The catalytic performance of ZnO$_2$ NPs for the reaction was therefore studied. Under identical reaction conditions (*i.e.*, 37.5 mg of ZnO$_2$ NPs, 5.87 mmol of H$_2$O$_2$, 5 mL of CH$_3$CN, and a propylene pressure of 20 bar at 50 °C for 6 h), it gave a PO yield of 85.12% (100% PO selectivity) and a PO productivity of 1290 mg h^{-1} g$_{cat}^{-1}$, with a TON of 14.4, a H$_2$O$_2$ conversion of 91.66%, and a H$_2$O$_2$ utilization efficiency of 92.86%. No conversion of propylene was observed when CH$_3$CN was replaced by water. Overall, the catalytic performance of ZnO$_2$ NPs is very similar to that of ZnO-NR (Entry 2 of Table 1 and Entry 1 of Table S1†). This strongly suggests that ZnO$_2$, formed from ZnO under reaction conditions, is the main catalytically active species for the epoxidation reaction.

This journal is © The Royal Society of Chemistry 2025

J. Mater. Chem. A, 2025, **13**, 5261–5274 | **5269**

The key role of H_2O_2 in the epoxidation of propylene over ZnO-based catalysts was further confirmed by reactions with ^{18}O-enriched oxidants. The catalytic reactions with $H_2{}^{18}O_2$ (conditions: 37.5 mg of ZnO-NR, 300 μL of the aqueous solution of 2.0–2.4% $H_2{}^{18}O_2$, 5 mL of CH_3CN, and a propylene pressure of 20 bar at 50 °C for 6 h) or with $H_2{}^{16}O_2$ and $^{18}O_2$ (conditions: 37.5 mg of ZnO-NR, 5.87 mmol of H_2O_2, 5 mL of CH_3CN, 20 bar of propylene pressure with ~5% $^{18}O_2$ at 50 °C for 6 h) were conducted and the resulting product of PO was analyzed by GC/MS. As shown in Fig. 7, no ^{18}O-enriched PO was detected for the reaction with $H_2{}^{16}O_2$ and $^{18}O_2$, while an enrichment of 72% was observed for the reaction with $H_2{}^{18}O_2$, with roughly one-to-one stoichiometry of H_2O_2 and PO. The results indicated that the ZnO-based catalysts reacted with H_2O_2 but not with O_2 to generate reactive oxygenated species to further react with propylene to produce PO.

The HPPO process over ZnO-based catalysts should be associated with the reactive species in the ZnO_2 NPs formed upon the reaction of ZnO with H_2O_2. Selected catalysts were further analyzed by EPR and XPS to probe and investigate the possible reactive species. The EPR spectra of fresh and spent catalysts of ZnO-NR and ZnO/MCM-41(7.99) as well as the spectrum of ZnO_2 NPs were recorded at 77 K. In principle, both ZnO and ZnO_2 are EPR silent, but the peroxide (O_2^{2-}) ions on ZnO_2 may react with water to form EPR-active superoxide (O_2^-) species.[40] As shown in Fig. 8a, while the fresh catalysts did not show any signals in their spectra, the spectrum of ZnO_2 NPs displayed an axial peak at $g_\parallel \sim 2.030$ and $g_\perp \sim 2.000$, where the perpendicular absorption linewidth is large so that the difference between g_{yy} and g_{xx} cannot be significantly resolved. The corresponding results further supported the presence of superoxide species adsorbed to Zn^{2+} in the sample.[40,41,60] The signals were also observed for the two spent catalysts. The integration intensity ratio for ZnO-NR$_{sp}$, ZnO/MCM-41(7.99)$_{sp}$, and ZnO_2 NP was determined to be 1.0 : 1.0 : 2.0 (Fig. S8†). Interestingly, the Zn species with a relatively small amount (7.99%) in ZnO/MCM-41(7.99)$_{sp}$ resulted in comparable spin intensity (no signal of the MCM-41-only material) for paramagnetic superoxide species, implying the role of the mesoporous materials in assisting the dispersion and storage of the reactive species in the composite. The comparable values of PO productivity (P_{PO}, per gram of catalyst) for ZnO-NR and ZnO/
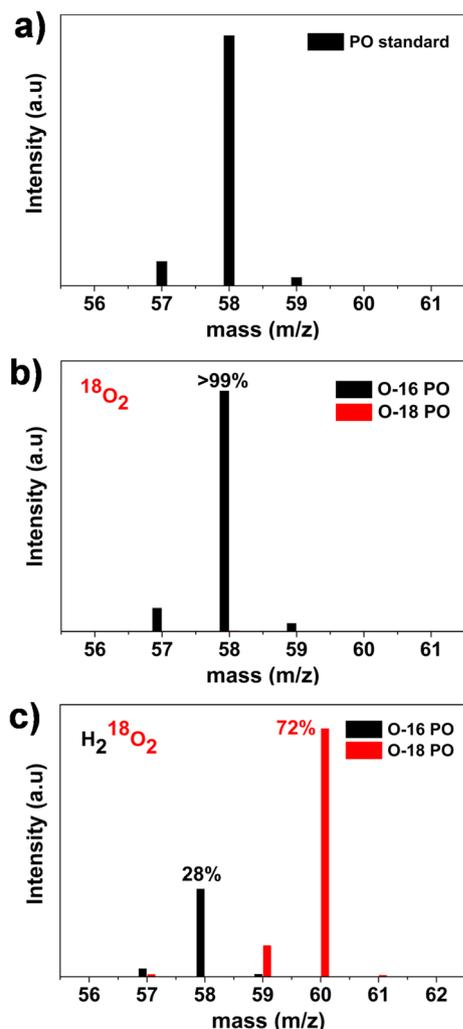

Fig. 7 The MS data of propylene epoxidation over ZnO-NR with (a) $H_2{}^{16}O_2$, (b) $^{18}O_2$ (97 atom%) and $H_2{}^{16}O_2$, and (c) $H_2{}^{18}O_2$ (90 atom%, 2.0–2.4% aqueous solution).
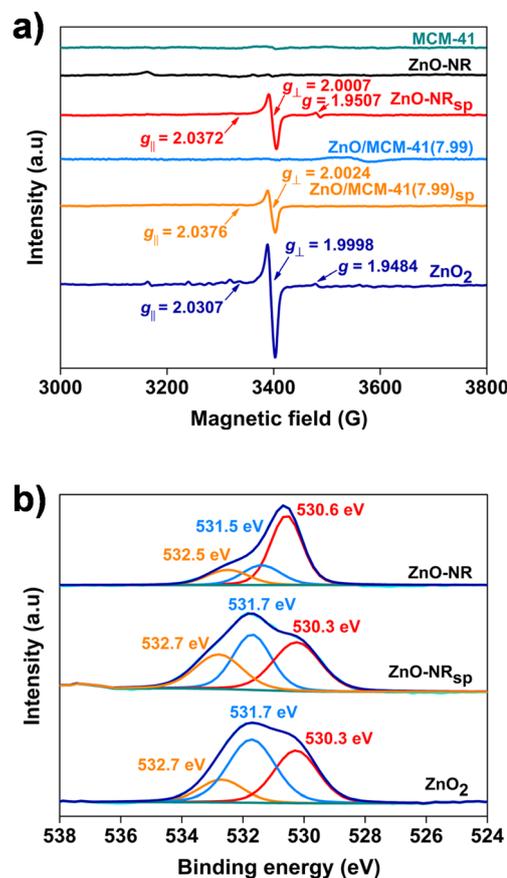

Fig. 8 (a) EPR spectra of MCM-41, ZnO-NR, ZnO-NR$_{sp}$, ZnO/MCM-41(7.99), ZnO/MCM-41(7.99)$_{sp}$, and ZnO_2 NPs measured at 77 K. (b) O 1s XPS spectra and deconvoluted peaks of ZnO-NR, ZnO-NR$_{sp}$, and ZnO_2 NPs.

5270 | J. Mater. Chem. A, 2025, 13, 5261–5274

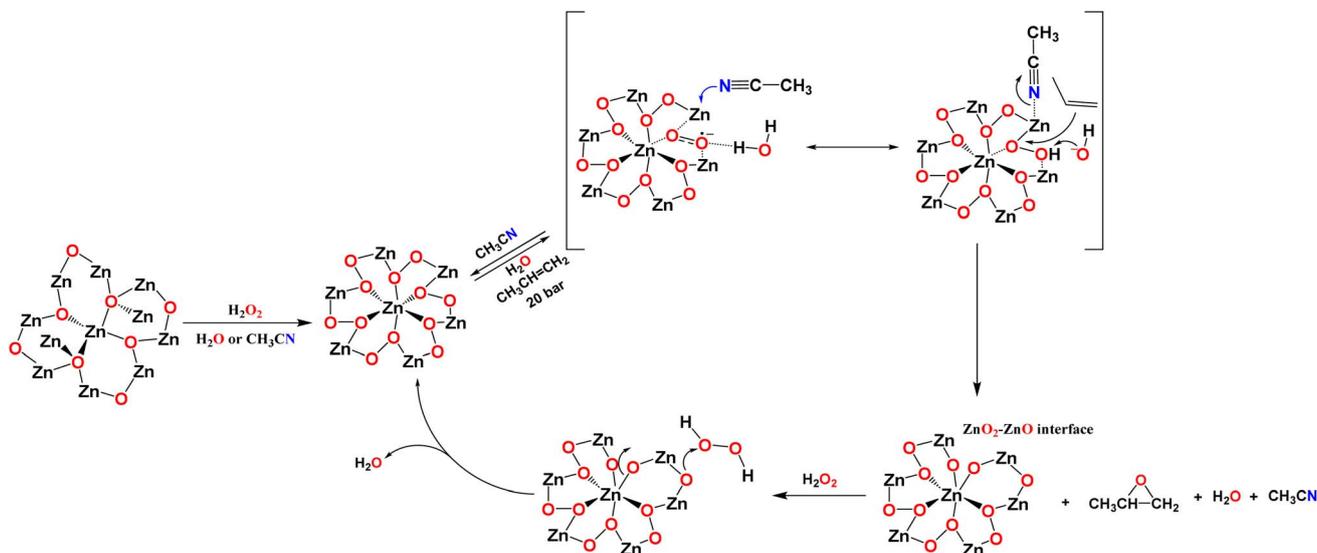This journal is © The Royal Society of Chemistry 2025

MCM-41(7.99) further support this point (Table S1†). For ZnO-NR_{sp} and ZnO_2 NPs, the additional signal at $g \sim 1.95$, which could be attributed to the oxygen vacancy with trapped electrons,[40,61,62] was also observed. Since water was present in the reaction media for all the catalytic tests, one could conclude that both peroxide and superoxide species should be present in the ZnO-based catalysts in the HPPO process. The peroxide and superoxide species were thermally stable up to 200 °C and were converted to O_2 at 210–250 °C, as revealed by analysis of TGA-GC/MS (Fig. S9†).

XPS was further applied to probe the binding energy (BE) and chemical state of oxygen-containing species on the surface of these catalysts. The O 1s spectra of the fresh and spent catalysts and ZnO_2 NPs are shown in Fig. 8b and S10.† The spectrum of ZnO-NR can be deconvoluted into three peaks at ~530.6, 531.5, and 532.5 eV, corresponding to the O^{2-} anions in the lattice (O_L), the oxygen anions (O_x^-) in the vicinity of oxygen vacancies (V_O), and the chemisorbed O_2 or H_2O (O_C), respectively.[63,64] The values of BE for V_O and O_C are characteristic of defect-rich oxides.[65] Similarly, the spectrum of ZnO/MCM-41(7.99) was fitted with the contributions of the three species (Fig. S10†), with a much more intense peak at 532.6 eV mainly attributed to the framework oxygen (Si–O–Si/Al) of MCM-41 as well as the surface OH groups and the O_C on ZnO-NR.[53,66] For ZnO_2 NPs, on the other hand, its spectrum can be well fitted with three components (Fig. 8b). The most intense peak at 531.7 eV should be mainly attributed to both the O_2^{2-} anions (and related hydroperoxide, OOH^-) of ZnO_2 as well as the EPR-active superoxide species on the surface.[63,64] The presence of V_O species, as suggested by EPR, might also contribute to the peak. The other two peaks at 530.3 and 532.7 eV are relatively weak and they are assigned to the O^{2-} anions of ZnO, possibly formed by the decomposition of ZnO_2[59] and the chemisorbed species (O_C), respectively. The spectrum of the spent catalyst ZnO-NR_{sp} resembles that of ZnO_2, with the values of BE of the three fitted

peaks being identical to those for ZnO_2. Comparing the relative intensities of the three peaks suggests that ZnO-NR_{sp} possessed fewer peroxide (and hydroperoxide), superoxide, and V_O species, yet more O_C on its surface than ZnO_2 did. Similar changes in the surface species were also observed for ZnO/MCM-41(7.99)$_{sp}$ after catalytic reaction (Fig. S10†).

Based on our findings, we propose a catalytic cycle for the HPPO process over ZnO-based catalysts with acetonitrile as a solvent. As shown in Scheme 1, under the reaction conditions, the hexagonal ZnO-NR first reacts with H_2O_2 to transform the four-coordinated Zn^{2+} cations with tetrahedral geometry to the six-coordinated octahedral Zn centers of cubic ZnO_2. The process can store additional oxygen atoms from H_2O_2 with the reactive species anchored at the Zn centers. The Zn-peroxide species may react with water to form EPR-active Zn-superoxide species and may also generate related Zn-hydroperoxide species (suggested by XPS) on ZnO_2. All these species may be capable of epoxidizing propylene via a direct O-atom transfer reaction[6] with the assistance of acetonitrile and a nearby aqueous hydrogen bonding network. The acetonitrile molecule may serve as a decent ligand[33,67] to coordinate and interact with Zn^{2+} through the nitrogen atom and open up the Zn–O coordination during the catalytic cycle for O-atom transfer to the olefin to selectively produce PO. The coordination and geometry of the proposed intermediate states might resemble those in TS-1 catalysts.[5,6] Moreover, the presence of a nearby water molecule can be essential for forming the H-bonding network to activate the peroxide (and other reactive species) and enable epoxidation. In our study, acetonitrile was the solvent and the water molecules needed for the proposed catalytic cycle came from the aqueous solution of H_2O_2. Such reaction conditions seemed to be necessary, noting that the corresponding chemistry cannot be conducted in a protic solvent of methanol or an aqueous environment. After forming PO, the Zn center within a six-membered ring of $(ZnO)_3$, resembling the structure of ZnO,

Scheme 1 A proposed mechanism for the HPPO process over ZnO-NR with H_2O_2 in CH_3CN.

This journal is © The Royal Society of Chemistry 2025

J. Mater. Chem. A, 2025, **13**, 5261–5274 | **5271**

may further react with another molecule of H_2O_2 to regenerate the active site on ZnO_2, forming one molecule of water as a byproduct. It is noted that similar species of peroxide, hydroperoxide and superoxide were also detected for olefinic epoxidation and aromatic hydroxylation with H_2O_2 over TS-1 and TiMCM-41.[68–70] In our study, the results of XAS and nitrogen physisorption reveal that the dispersion of ZnO by MCM-41 is beneficial for forming and accumulating more (up to 84%) reactive ZnO_2 in the spent ZnO/MCM-41(7.99) catalyst. With the assistance of acetonitrile, an aprotic polar organic solvent, the hydrophobic propylene substrate may diffuse into the mesopores of MCM-41 and may also approach the active sites on ZnO_2 more easily with reduced activation free energy due to enthalpy–entropy compensation.[20] We could thus bridge the microscopic properties and the macroscopic catalytic performance for the HPPO process over highly active ZnO/ZnO_2 catalysts.[71–73] Finally, the fact that no amide or organic peroxide was detected in our catalytic studies strongly suggests that an organic peroxide process was not involved in the HPPO process over the ZnO-based catalysts.

4 Conclusions

ZnO-based catalysts, including ZnO-NR and ZnO/MCM-41(*x*) composites, have been prepared and applied for the epoxidation of propylene with H_2O_2 in acetonitrile under low temperatures (30–70 °C) and high pressures (5–20 bar). The ZnO catalysts exhibited high epoxidation activity with high H_2O_2 utilization and PO selectivity. The amount of ZnO in ZnO/MCM-41(*x*) composites has been optimized to give ≥98% H_2O_2 utilization and nearly 100% PO selectivity. The catalytic performance of the ZnO-based catalysts is comparable to that of TS-1 catalysts under similar reaction conditions. Moreover, ZnO_2 has been identified as forming from the reaction of ZnO with H_2O_2 and served as a novel green oxygen-storage oxide material. The reactive species on ZnO_2, including peroxide, hydroperoxide, and superoxide, are proposed to epoxidize propylene through a direct O-atom transfer reaction with the assistance of acetonitrile and a nearby aqueous hydrogen bonding network. The ZnO-based catalytic system with H_2O_2 in acetonitrile shows high efficiency and recyclability and may be promising for practical applications.

Data availability

The authors confirm that the data supporting the findings of this study are within the article and ESI.†

Author contributions

Gebretinsae Yeabyo Nigussie: data collection, methodology, conceptualization, data analysis, writing – original draft, review, and editing. Yi-Fang Tsai: data collection, conceptualization, and methodology. Tsung-Cheng Yang: data collection and methodology. Chia-Min Yang: funding acquisition, supervision, conceptualization, methodology, data analysis, investigation, writing – original draft, review and editing. Steve S.-F. Yu:

funding acquisition, supervision, conceptualization, methodology, data analysis, investigation, writing – original draft, review and editing.

Conflicts of interest

There is no conflict of interest to declare.

Acknowledgements

References

1 J. Herzberger, K. Niederer, H. Pohlit, J. Seiwert, M. Worm, F. R. Wurm and H. Frey, *Chem. Rev.*, 2016, **116**, 2170–2243.

2 J. Teržan, M. Huš, B. Likozar and P. Djinović, *ACS Catal.*, 2020, **10**, 13415–13436.

3 J. Tsuji, J. Yamamoto, M. Ishino and N. Oku, *Sumitomo Kagaku*, 2006, **1**, 4–10.

4 Q. Hua, T. Cao, X. K. Gu, J. Lu, Z. Jiang, X. Pan, L. Luo, W. X. Li and W. Huang, *Angew. Chem., Int. Ed.*, 2014, **126**, 4956–4961.

5 V. Russo, R. Tesser, E. Santacesaria and M. Di Serio, *Ind. Eng. Chem. Res.*, 2013, **52**, 1168–1178.

6 V. Smeets, E. M. Gaigneaux and D. P. Debecker, *ChemCatChem*, 2022, **14**, e202101132.

7 A. S. Sharma, V. S. Sharma, H. Kaur and R. S. Varma, *Green Chem.*, 2020, **22**, 5902–5936.

8 J. Yamamoto, C. Works, H. Koike and S. Yoshida, *Sumitomo Kagaku Report*, 2019, 1–9.

9 J. Wei, S. Wang, J. Wu, D. Cao and D. Cheng, *Ind. Chem. Mater.*, 2024, **2**, 7–29.

10 J. M. Campos-Martin, G. Blanco-Brieva and J. L. Fierro, *Angew. Chem., Int. Ed.*, 2006, **45**, 6962–6984.

11 J. Z. Tan, D. T. Bregante, C. Torres and D. W. Flaherty, *J. Catal.*, 2022, **405**, 91–104.

12 M. Alvear, C. Schmidt, O. Reinsdorf, E. Lebron-Rodriguez, A. Al Abdulghani, I. Hermans, M. Peurla, M. Lastusaari, K. Eränen and D. Y. Murzin, *Catal. Lett.*, 2023, 1–12.

5272 | *J. Mater. Chem. A*, 2025, **13**, 5261–5274

This journal is © The Royal Society of Chemistry 2025

13 W. Li, L. Chen, M. Qiu, W. Li, Y. Zhang, Y. Zhu, J. Li and X. Chen, *ACS Catal.*, 2023, **13**, 10487–10499.

14 C. Miao, N. He, Q. Zhu, Y. Yi, Z. Feng and H. Guo, *Catal. Lett.*, 2020, **150**, 281–290.

15 N. Sheng, Z. Liu, Z. Song, D. Lin, X. Feng, Y. Liu, X. Chen, D. Chen, X. Zhou and C. Yang, *Chem. Eng. J.*, 2019, **377**, 119954.

16 Z. Song, X. Feng, N. Sheng, D. Lin, Y. Li, Y. Liu, X. Chen, X. Zhou, D. Chen and C. Yang, *Catal. Today*, 2020, **347**, 102–109.

17 A. Pulido, P. Concepción, M. Boronat and A. Corma, *J. Catal.*, 2012, **292**, 138–147.

18 E. J. Lee, J. Lee, M. Lee, H.-K. Min, S. Park and D. H. Kim, *Mol. Catal.*, 2019, **467**, 111–119.

19 Y. Yu, N. Fang, Z. Chen, D. Liu, Y. Liu and M. He, *ACS Sustainable Chem. Eng.*, 2022, **10**, 11641–11654.

20 D. S. Potts, D. T. Bregante, J. S. Adams, C. Torres and D. W. Flaherty, *Chem. Soc. Rev.*, 2021, **50**, 12308–12337.

21 X. Liu, X. Wang, X. Guo and G. Li, *Catal. Today*, 2004, **93**, 505–509.

22 X. Nie, X. Ji, Y. Chen, X. Guo and C. Song, *Mol. Catal.*, 2017, **441**, 150–167.

23 G. Bellussi, A. Carati, M. G. Clerici, G. Maddinelli and R. Millini, *J. Catal.*, 1992, **133**, 220–230.

24 Q. Qin, H. Liu, Y. Guo, B. Wang, J. Zhu and J. Ma, *Phys. Chem. Chem. Phys.*, 2023, **25**, 21358–21375.

25 F. Song, Y. Liu, L. Wang, H. Zhang, M. He and P. Wu, *Stud. Surf. Sci. Catal.*, 2007, **170**, 1236–1243.

26 X. Lu, H. Wu, J. Jiang, M. He and P. Wu, *J. Catal.*, 2016, **342**, 173–183.

27 J. Yin, X. Jin, H. Xu, Y. Guan, R. Peng, L. Chen, J. Jiang and P. Wu, *Chin. J. Catal.*, 2021, **42**, 1561–1575.

28 G. Laus, *J. Chem. Soc., Perkin Trans. 2*, 2001, 864–868.

29 T. Mallat and A. Baiker, *Catal. Sci. Technol.*, 2011, **1**, 1572–1583.

30 L. Wu, X. Deng, S. Zhao, H. Yin, Z. Zhuo, X. Fang, Y. Liu and M. He, *Chem. Commun.*, 2016, **52**, 8679–8682.

31 D. Pan, L. Kong, H. Zhang, Y. Zhang and Y. Tang, *ACS Appl. Mater. Interfaces*, 2023, **15**, 28125–28134.

32 Y. Wang, H. Yang, Y. Zuo, D. Tian, G. Hou, Y. Su, Z. Feng, X. Guo and C. Li, *Appl. Catal., B*, 2023, **325**, 122396.

33 Y.-J. Lu, D. Janmanchi, T. Natarajan, Z.-H. Lin, W. H. Wanna, I.-J. Hsu, D.-L. M. Tzou, T. Ayalew Abay and S. S.-F. Yu, *ChemCatChem*, 2022, **14**, e202200030.

34 D. T. Bregante, A. M. Johnson, A. Y. Patel, E. Z. Ayla, M. J. Cordon, B. C. Bukowski, J. Greeley, R. Gounder and D. W. Flaherty, *J. Am. Chem. Soc.*, 2019, **141**, 7302–7319.

35 S. K. Maiti, A. Ramanathan and B. Subramaniam, *Ind. Eng. Chem. Res.*, 2019, **58**, 17727–17735.

36 D. T. Bregante, N. E. Thornburg, J. M. Notestein and D. W. Flaherty, *ACS Catal.*, 2018, **8**, 2995–3010.

37 A. Kołodziejczak-Radzimska and T. Jesionowski, *Materials*, 2014, 7, 2833–2881.

38 Z. Mirzaeifard, Z. Shariatinia, M. Jourshabani and S. M. Rezaei Darvishi, *Ind. Eng. Chem. Res.*, 2020, **59**, 15894–15911.

39 D. Bocharov, A. Chesnokov, G. Chikvaidze, J. Gabrusenoks, R. Ignatans, R. Kalendarev, M. Krack, K. Kundzins, A. Kuzmin and N. Mironova-Ulmane, *J. Phys. Chem. Solids*, 2022, **160**, 110318.

40 R. Iyengar and V. S. Rao, *J. Phys. Chem. C*, 1971, **75**, 3089–3092.

41 A. I. Shames, O. Lev, A. A. Mikhaylov, A. G. Medvedev, J. Gun and P. V. Prikhodchenko, *J. Phys. Chem. C*, 2019, **123**, 20884–20892.

42 S. Verma and S. L. Jain, *Inorg. Chem. Front.*, 2014, **1**, 534–539.

43 S. Chawla, H. Uppal, M. Yadav, N. Bahadur and N. Singh, *Ecotoxicol. Environ. Saf.*, 2017, **135**, 68–74.

44 D. A. Giannakoudakis, M. Florent, R. Wallace, J. Secor, C. Karwacki and T. J. Bandosz, *Appl. Catal., B*, 2018, **226**, 429–440.

45 M. Hosseini-Sarvari and Z. Bazyar, *ChemistrySelect*, 2020, **5**, 8853–8857.

46 D. G. Montjoy, E. A. Wilson, H. Hou, J. D. Graves and N. A. Kotov, *Nat. Commun.*, 2023, **14**, 857.

47 V. Arca, A. B. Boscoletto, N. Fracasso, L. Meda and G. Ranghino, *J. Mol. Catal. A: Chem.*, 2006, **243**, 264–277.

48 P. Ghasemipour, M. Fattahi, B. Rasekh and F. Yazdian, *Sci. Rep.*, 2020, **10**, 4414.

49 D. Liu, L. Cao, G. Zhang, L. Zhao, J. Gao and C. Xu, *Fuel Process. Technol.*, 2021, **216**, 106770.

50 R. Al-Gaashani, S. Radiman, A. Daud, N. Tabet and Y. Al-Douri, *Ceram. Int.*, 2013, **39**, 2283–2292.

51 V. Alvarado-Pérez, L. I. Cabrera-Lara, G. López-Téllez, D. Mendoza-Anaya, S. Hernández-López and M. Camacho-López, *Mater. Chem. Phys.*, 2019, **233**, 180–184.

52 R. M. Sellers, *Analyst*, 1980, **105**, 950–954.

53 Z. Zhou, Y. Wu, H. Ling, J. Guo, S. Wang and M. Li, *J. Ind. Eng. Chem.*, 2023, **119**, 218–225.

54 V. Russo, R. Tesser, E. Santacesaria and M. Di Serio, *Ind. Eng. Chem. Res.*, 2014, **53**, 6274–6287.

55 W. Cheng, X. Wang, G. Li, X. Guo and S. Zhang, *J. Catal.*, 2008, **255**, 343–346.

56 B. Liu and H. C. Zeng, *J. Am. Chem. Soc.*, 2003, **125**, 4430–4431.

57 J. S. Beck, J. C. Vartuli, W. J. Roth, M. E. Leonowicz, C. Kresge, K. Schmitt, C. Chu, D. H. Olson, E. Sheppard and S. McCullen, *J. Am. Chem. Soc.*, 1992, **114**, 10834–10843.

58 K. M. McPeak, M. A. Becker, N. G. Britton, H. Majidi, B. A. Bunker and J. B. Baxter, *Chem. Mater.*, 2010, **22**, 6162–6170.

59 T. Daley, K. B. Opuni, E. Raj, A. J. Dent, G. Cibin, T. I. Hyde and G. Sankar, *J. Phys.: Condens. Matter*, 2021, **33**, 264002.

60 M. Che and A. J. Tench, *Adv. Catal.*, 1983, **32**, 1–148.

61 M. Buryi, V. Babin, Y. Y. Chang, Z. Remeš, J. Mičová and D. Šimek, *Appl. Surf. Sci.*, 2020, **525**, 146448.

62 A. B. Djurišić, Y. H. Leung, W. C. H. Choy, K. W. Cheah and W. K. Chan, *Appl. Phys. Lett.*, 2004, **84**, 2635–2637.

63 Z. Geng, X. Kong, W. Chen, H. Su, Y. Liu, F. Cai, G. Wang and J. Zeng, *Angew. Chem., Int. Ed.*, 2018, **130**, 6162–6167.

64 H. Yuan, S. A. A. A. Aljneibi, J. Yuan, Y. Wang, H. Liu, J. Fang, C. Tang, X. Yan, H. Cai and Y. Gu, *Adv. Mater.*, 2019, **31**, 1807161.

This journal is © The Royal Society of Chemistry 2025

J. Mater. Chem. A, 2025, **13**, 5261–5274 | **5273**

65 K. Banger, Y. Yamashita, K. Mori, R. Peterson, T. Leedham, J. Rickard and H. Sirringhaus, *Nat. Mater.*, 2011, **10**, 45–50.

66 C. Miao, K. Shang, L. Liang, S. Chen and J. Ouyang, *ACS Sustain. Chem. Eng.*, 2022, **10**, 12771–12782.

67 S. F. Rach and F. E. Kühn, *Chem. Rev.*, 2009, **109**, 2061–2080.

68 Q. Zhao, X.-H. Bao, Y. Wang, L.-W. Lin, G. Li, X.-W. Guo and X.-S. Wang, *J. Mol. Catal. A: Chem.*, 2000, **157**, 265–268.

69 K. Chaudhari, D. Srinivas and P. Ratnasamy, *J. Catal.*, 2001, **203**, 25–32.

70 D. Srinivas, P. Manikandan, S. C. Laha, R. Kumar and P. Ratnasamy, *J. Catal.*, 2003, **217**, 160–171.

71 W. Chen, G. Qian, Y. Wan, D. Chen, X. Zhou, W. Yuan and X. Duan, *Acc. Chem. Res.*, 2022, **55**, 3230–3241.

72 X. Zhang, N. Fei, Q. Wang, A. R. Khan, W. Chen, G. Qian, J. Zhang, D. Chen, X. Duan, X. Zhou and W. Yuan, *J. Mater. Chem. A*, 2024, **12**, 21884–21894.

73 W. Chen, W. Fu, X. Duan, B. Chen, G. Qian, R. Si, X. Zhou, W. Yuan and D. Chen, *Engineering*, 2022, **14**, 124–133.

5274 | *J. Mater. Chem. A*, 2025, **13**, 5261–5274

This journal is © The Royal Society of Chemistry 2025